Frontiers of Physics
https://doi.org/10.1007/s11467-021-1127-0
Front. Phys.
17(3), 32503 (2022)

RESEARCH ARTICLE

Kink-like breathers in Bose–Einstein condensates with helicoidal spin–orbit coupling

Yixin Yang[1,2], **Peng Gao**[1,2], **Li-Chen Zhao**[1,2,3], **Zhan-Ying Yang** [1,2,3,†]

[1] *School of Physics, Northwest University, Xi'an 710127, China*
[2] *Shaanxi Key Laboratory for Theoretical Physics Frontiers, Xi'an 710127, China*
[3] *Peng Huanwu Center for Fundamental Theory, Xi'an 710127, China*
Corresponding author. E-mail: [†] *zyyang@nwu.edu.cn*
Received July 17, 2021; accepted September 24, 2021

We report a kind of kink-like breathers in one-dimensional Bose–Einstein condensates (BECs) with helicoidal spin–orbit coupling (SOC), on whose two sides the background densities manifest obvious difference (called kink amplitude). The kink amplitude and shape of breather can be adjusted by the strength and period of helicoidal SOC, and its atomic number in two components exchanges periodically with time. The SOC has similar influence on the kink amplitude and the exchanged atomic number, especially when the background wave number is fixed. It indicates that the oscillating intensity of breather can be controlled by adjusting initial kink amplitude. Our work showcases the great potential of realizing novel types of breathers through SOC, and deepens our understanding on the formation mechanisms of breathers in BECs.

Keywords Bose–Einstein condensates, spin–orbit coupling, breather

1 Introduction

Breather is an important kind of nonlinear waves, which have attracted broad attention over the last few years. It includes two main categories according to its different background wave, namely, on-zero-background breathers (also called breathing solitons) [1–3] and on-plane-wave ones [4–10]. The former manifests the oscillation around equilibrium of lowest energy; the latter is formed by the interference between background and perturbation (it is the key object of our study so is briefly called "breather" in the rest of this paper). According to the property of breathing, breathers can be classified into many species, such as Kuznetsov–Ma breather (KMB) [4, 5], Akhmediev breather (AB) [6], Tajiri–Watanabe breathers (TWB) [7], and even super-regular breather [8–10]. These waves can exist broadly in various physical systems, such as nonlinear optical fibers, Bose–Einstein condensates (BECs), plasma, and water [1, 2, 11–16]. Meanwhile, the diversity of their structures is attracting considerable interest,such as the breather with anti-eye and four-petal shape, which has been constructed in multi-component systems [17]. Moreover, their superposition can lead to the distinct chessboard-like structure and inelastic collisions [17, 18].

Numerous works mentioned above were devoted to the research of different breather structures and their characteristics, which implies that the discovery of new breather structures is a matter of great concern. Ultracold Bose gas is an ideal platform for the study of nonlinear waves including solitons and breathers, and the effect of spin–orbit coupling (SOC) plays a vital role in adjusting the structure of waves [19–27]. Recently, the SOC with helicoidal spatial modulation in BECs was reported in Ref. [28]. This system has a more superior controllability and more flexible adjustability than the ordinary SOC systems [22, 29–33]. Thus, it is natural to wonder if the system can bring new structures and physical characters for breathers.

In this paper, we study the breathers in BECs with helicoidal SOC. The exact analytical solution is obtained through the Darboux transformation method and the transformation between Gross–Pitaevskii equation (GPE) and the Manakov system. As we discover below, there is the kink-like breather when the background wave number is connected to the momentum minima of system's lowest energy states, and the helicoidal SOC can influence the shape of kink-like breather. Taking the first component as an example, the breather's one valley gradually splits into two valleys with the strength of SOC increasing. Meanwhile, the kink amplitude can be adjusted by the strength and period of the helicoidal SOC, and an unexpected jump occurs in this process. Also, we test the atomic number oscillation characteristics of the kink-like breather. Interestingly, the helicoidal SOC exhibits simi-

* This article can also be found at http://journal.hep.com.cn/fop/EN/10.1007/s11467-021-1127-0.

lar effects on the atomic number oscillating amplitude as well as kink amplitude, especially when background wave number is fixed. In addition, there is also an unexpected jump when the atomic number changes with helicoidal SOC. These results also suit for the second component.

2 Models and breather solution

The dynamics of BECs with helicoidal SOC is described by the following GPE [28]:

$$\mathrm{i}\frac{\partial \boldsymbol{\Psi}}{\partial t} = \frac{1}{2}\left[-\mathrm{i}\frac{\partial}{\partial x} + \alpha \boldsymbol{A}(x)\right]^2 \boldsymbol{\Psi} - g(\boldsymbol{\Psi}^\dagger \boldsymbol{\Psi})\boldsymbol{\Psi}, \tag{1}$$

where $\boldsymbol{\Psi} = (\psi_1, \psi_2)^{\mathrm{T}}$ is the spinor wave function, ψ_1 for spin-up and ψ_2 for spin-down. And $\boldsymbol{A}(x) = \boldsymbol{\sigma}\boldsymbol{n}(x)$ refers to the helicoidal gauge potential. The position-dependent unit vector $\boldsymbol{n}(x) = [\cos(2\kappa x), \sin(2\kappa x), 0]$ determines the SOC direction with period π/κ and rotation frequency 2κ. This setting can be implemented by an appropriate optical lattice, which determines the helicoidal SOC structure [34, 35]. The strength of SOC, α, is experimentally tunable [36, 37], and $\boldsymbol{\sigma} = (\sigma_x, \sigma_y, \sigma_z)$ are the Pauli matrices. $g(\boldsymbol{\Psi}^\dagger\boldsymbol{\Psi})\boldsymbol{\Psi}$ denotes interatomic interactions, inter- and intraspecies interactions are equal for simplicity, and $g > 0$ (or $g < 0$) means attractive(or repulsive) interatomic interactions. We use the units with $m = \hbar = 1$, and $g = 1$. Specially, when $\kappa = 0$, the helicoidal gauge potential will reduce to uniform potential (Rashba–Dresslhaus coupling scheme [29, 30]).

In fact, there is a transformation between the GPE and Manakov system [28, 38],

$$\mathrm{i}\boldsymbol{u}_t + (1/2)\boldsymbol{u}_{xx} + (\boldsymbol{u}^\dagger\boldsymbol{u})\boldsymbol{u} = 0, \tag{2}$$

where $\boldsymbol{u} = (u_1, u_2)^{\mathrm{T}}$. Enlighted by the results of Refs. [28, 39], one can assume

$$\begin{aligned}\boldsymbol{\Psi}_1 &= -A\mathrm{e}^{-\mathrm{i}(k_{\min}+\kappa)x}u_1 - B\mathrm{e}^{\mathrm{i}(k_{\min}-\kappa)x}u_2,\\ \boldsymbol{\Psi}_2 &= B\mathrm{e}^{-\mathrm{i}(k_{\min}-\kappa)x}u_1 + A\mathrm{e}^{\mathrm{i}(k_{\min}+\kappa)x}u_2,\end{aligned} \tag{3}$$

where $A = -\sqrt{\frac{k_{\min}-\kappa}{2k_{\min}}}$, $B = \sqrt{\frac{k_{\min}+\kappa}{2k_{\min}}}$. $k_{\min} = \sqrt{\alpha^2+\kappa^2}$ is the corresponding momentum minimum of the lowest energy states in energy–quasimomentum dispersion, and the states near the minimum are dressed spin states [21]. Generally, in spin–orbit coupled BEC, the dispersion relation always shows the double-well structures [21, 24, 29]. And the dispersion relation of the BEC with helicoidal SOC also have the similar structures and degenerate lowest energy states [28, 40], $\pm k_{\min}$ is the quasimomentum values corresponding to the lowest energy in the dispersion relation. The ansatz (3) links two lowest energies states, so $k_{\min}$ plays a very important role in the transformation. Substituting the above ansatz (3) into Eq. (1), the GPE can be reduced to the well-known Manakov system. This means that the solution of Eq. (1) can be constructed through the solutions of Manakov system.

The breather solutions of Manakov system are obtained through the Darboux transformation, which is a very powerful method to construct exact solutions and transfer a nonlinear problem to a linear spectral one [41–47]. The corresponding Lax pair of Manakov system (2) can be represented by

$$\boldsymbol{\Phi}_x = \boldsymbol{U}(x,t;\lambda)\boldsymbol{\Phi}, \quad \boldsymbol{\Phi}_t = \boldsymbol{V}(x,t;\lambda)\boldsymbol{\Phi}, \tag{4}$$

where $\lambda = a + \mathrm{i}b$ is the spectral parameter, and $\boldsymbol{\Phi} = (\Phi_1, \Phi_2, \Phi_3)^{\mathrm{T}}$,

$$\boldsymbol{U} = \begin{pmatrix} -\mathrm{i}\frac{2}{3}\lambda & u_1 & u_2 \\ -u_1^* & \frac{\mathrm{i}}{3}\lambda & 0 \\ -u_2^* & 0 & \frac{\mathrm{i}}{3}\lambda \end{pmatrix},$$

$$\boldsymbol{V} = \boldsymbol{U}\lambda + \begin{pmatrix} \mathrm{i}|u_1|^2 + \mathrm{i}|u_2|^2 & \mathrm{i}u_{1x} & \mathrm{i}u_{2x} \\ \mathrm{i}u_{1x}^* & -\mathrm{i}|u_1|^2 & -\mathrm{i}u_2u_1^* \\ \mathrm{i}u_{2x}^* & -\mathrm{i}u_2^*u_1 & -\mathrm{i}|u_2|^2 \end{pmatrix}.$$

The star denotes the complex conjugate. The seed solutions are $u_{01} = s_1\mathrm{e}^{\mathrm{i}\theta_1}$, $u_{02} = s_2\mathrm{e}^{\mathrm{i}\theta_2}$, where $\theta_{1,2} = \omega_{1,2}t/2 - k_{1,2}x$, $\omega_{1,2} = 2g_1s_1^2 + 2g_2s_2^2 - k_{1,2}^2$. After linearizing and diagonalizing the matrices U, V into $U_d = \mathrm{diag}(\tau_{u1}, \tau_{u2}, \tau_{u3})$, $V_d = \mathrm{diag}(\tau_{v1}, \tau_{v2}, \tau_{v3})$ (all the diagonal elements in U_{ld}, V_{ld} are complex numbers associated with λ and $k_{1,2}$), the vector eigenfunctions of linear system are obtained to be

$$\boldsymbol{\Phi} = \begin{pmatrix}\phi_1\\ \phi_2\\ \phi_3\end{pmatrix} = \begin{pmatrix}\mathrm{e}^{\tau_{u1}x+\tau_{v1}t}\\ \mathrm{e}^{\tau_{u2}x+\tau_{v2}t}\\ \mathrm{e}^{\tau_{u3}x+\tau_{v3}t}\end{pmatrix}. \tag{5}$$

Then the breather solutions can be constructed through the following Darboux transformation,

$$\begin{aligned} u_1 &= u_{01} + \frac{(\lambda^* - \lambda_1)\Phi_1\Phi_2^*}{|\Phi_1|^2 + |\Phi_2|^2 + |\Phi_3|^2},\\ u_2 &= u_{02} + \frac{(\lambda^* - \lambda_1)\Phi_1\Phi_3^*}{|\Phi_1|^2 + |\Phi_2|^2 + |\Phi_3|^2}. \end{aligned} \tag{6}$$

The breather solution hence reads

$$\begin{aligned} u_1 &= s_1(1 + 2bp_1)\mathrm{e}^{\mathrm{i}\theta_1},\\ u_2 &= s_2(1 + 2bp_2)\mathrm{e}^{\mathrm{i}\theta_2}, \end{aligned} \tag{7}$$

where s_1, s_2 are the background amplitudes, and

$$\begin{aligned} p_0 &= \mathrm{e}^{\iota}T_1 + \mathrm{e}^{-\iota}T_2 + 2T_3\cos\beta + 2T_4\sin\beta,\\ p_1 &= \frac{\zeta_1 - \mathrm{i}\zeta_2}{\mathrm{e}^{\iota}T_1 + \mathrm{e}^{-\iota}T_2 + 2T_3\cos\beta + 2T_4\sin\beta},\\ p_2 &= \frac{\zeta_3 - \mathrm{i}\zeta_4}{\mathrm{e}^{\iota}T_1 + \mathrm{e}^{-\iota}T_2 + 2T_3\cos\beta + 2T_4\sin\beta}. \end{aligned}$$

This solution (7) of Manakov system can describe the AB, KM, TW and four-petal breathers, etc. After substituting

the solution (7) into the transformation (3), we obtain a breather solution in the BECs with helicoidal SOC,

$$\begin{aligned}\boldsymbol{\Psi}_1 &= -\{As_1(1+2bp_1)\mathrm{e}^{\mathrm{i}[\theta_1-(k_{\min}+\kappa)x]}\\ &\quad +Bs_2(1+2bp_2)\mathrm{e}^{\mathrm{i}[\theta_2+(k_{\min}-\kappa)x]}\}p_0^{-1},\\ \boldsymbol{\Psi}_2 &= \{Bs_1(1+2bp_1)\mathrm{e}^{\mathrm{i}[\theta_1-(k_{\min}-\kappa)x]}\\ &\quad +As_2(1+2bp_2)\mathrm{e}^{\mathrm{i}[\theta_2+(k_{\min}+\kappa)x]}\}p_0^{-1},\end{aligned} \tag{8}$$

where

$$\begin{aligned}\zeta_1 &= \mathrm{e}^{\iota}E_1+\mathrm{e}^{-\iota}E_2+(E_1+E_2)\cos\beta-(F_1-F_2)\sin\beta,\\ \zeta_2 &= \mathrm{e}^{\iota}F_1+\mathrm{e}^{-\iota}F_2+(E_1-E_2)\sin\beta+(F_1+F_2)\cos\beta,\\ \zeta_3 &= \mathrm{e}^{\iota}E_3+\mathrm{e}^{-\iota}E_4+(E_3+E_4)\cos\beta-(F_3-F_4)\sin\beta,\\ \zeta_4 &= \mathrm{e}^{\iota}F_3+\mathrm{e}^{-\iota}F_4+(F_3+F_4)\cos\beta+(E_3-E_4)\sin\beta,\end{aligned}$$

and the symbols E_j, F_j, Ω_j, Δ_j are the polynomial with respect to λ, $s_{1,2}$, and $k_{1,2}$. Other variables are

$$\begin{aligned}&E_1=-\frac{3\chi_1}{\chi_1^2+\chi_3^2},\quad E_2=-\frac{3\chi_2}{\chi_2^2+\chi_5^2},\quad E_3=-\frac{3\chi_1}{\chi_1^2+\chi_4^2},\\ &F_1=-\frac{3\chi_3}{\chi_1^2+\chi_3^2},\quad F_2=-\frac{3\chi_5}{\chi_2^2+\chi_5^2},\quad F_3=-\frac{3\chi_4}{\chi_1^2+\chi_4^2},\\ &F_4=-\frac{3\chi_6}{\chi_2^2+\chi_6^2},\quad E_4=-\frac{3\chi_2}{\chi_2^2+\chi_6^2},\\ &\iota=mx+Mt/2+\alpha_0,\quad \beta=nx+Nt/2+\beta_0,\\ &T_1=1+(E_1^2+F_1^2)g_1s_1^2+(E_3^2+F_3^2)g_2s_2^2,\\ &T_2=1+(E_2^2+F_2^2)g_1s_1^2+(E_4^2+F_4^2)g_2s_2^2,\\ &T_3=1+(E_1E_2+F_1F_2)g_1s_1^2+(E_3E_4+F_3F_4)g_2s_2^2,\\ &T_4=(-E_2F_1+E_1F_2)g_1s_1^2+(-E_4F_3+E_3F_4)g_2s_2^2,\end{aligned}$$

and

$$\begin{aligned}&m=m_1-m_2,\ n=n_1-n_2,\ N=(m\kappa_3-n\kappa_4)/3,\\ &M=2(am-bn-m_1\kappa_1+m_2\kappa_2)/3,\\ &\kappa_1=3n_1-(k_1+k_2),\ \kappa_2=3n_2-(k_1+k_2),\\ &\kappa_4=-2a+3(n_1+n_2)-2(k_1+k_2),\\ &\chi_1=b+3m_1,\ \chi_2=b+3m_2,\ \chi_3=a-3n_1-2k_1+k_2,\\ &\chi_4=a-3n_1+k_1-2k_2,\ \chi_5=a-3n_2-2k_1+k_2,\\ &\kappa_3=2b+3(m_1+m_2),\ \chi_6=a-3n_2+k_1-2k_2,\\ &m_1=\mathrm{Re}[\tau_1],\ m_2=\mathrm{Re}[\tau_2],\ m_3=\mathrm{Re}[\tau_3],\\ &n_1=\mathrm{Im}[\tau_1],\ n_2=\mathrm{Im}[\tau_2],\ n_3=\mathrm{Im}[\tau_3],\end{aligned}$$

where

$$\begin{aligned}\tau_1 &= (-2\times3^{1/3}a_1+2^{1/3}C^{2/3})/(6^{2/3}C^{1/3}),\\ \tau_2 &= [2(3\mathrm{i}+\sqrt{3})a_1+\mathrm{i}\,2^{1/3}\times3^{1/6}(\mathrm{i}+\sqrt{3})C^{2/3}]\\ &\quad\times(2\times2^{2/3}\times3^{5/6}C^{1/3})^{-1},\\ \tau_3 &= [2(-3\mathrm{i}+\sqrt{3})a_1-2^{1/3}3^{1/6}(1+\mathrm{i}\sqrt{3})C^{2/3}]\\ &\quad\times(2\times2^{2/3}\times3^{5/6}C^{1/3})^{-1},\\ C &= \sqrt{12a_1^3+81b_1^2}-9b_1,\\ a_1 &= [\lambda^2-k_1(\lambda+k_1)-(\lambda+k_1)k_2+k_2^2]/3+g_1s_1^2+g_2s_2^2,\\ b_1 &= -\mathrm{i}[9g_2s_2^2+(\lambda+k_1-2k_2)(2\lambda-k_1-k_2)]\\ &\quad\times(\lambda-2k_1+k_2)/27-\mathrm{i}g_1s_1^2(\lambda+k_1-2k_2)/3.\end{aligned}$$

In general, the solution (8) represents breather structures on the periodic-wave background, and the kink-like

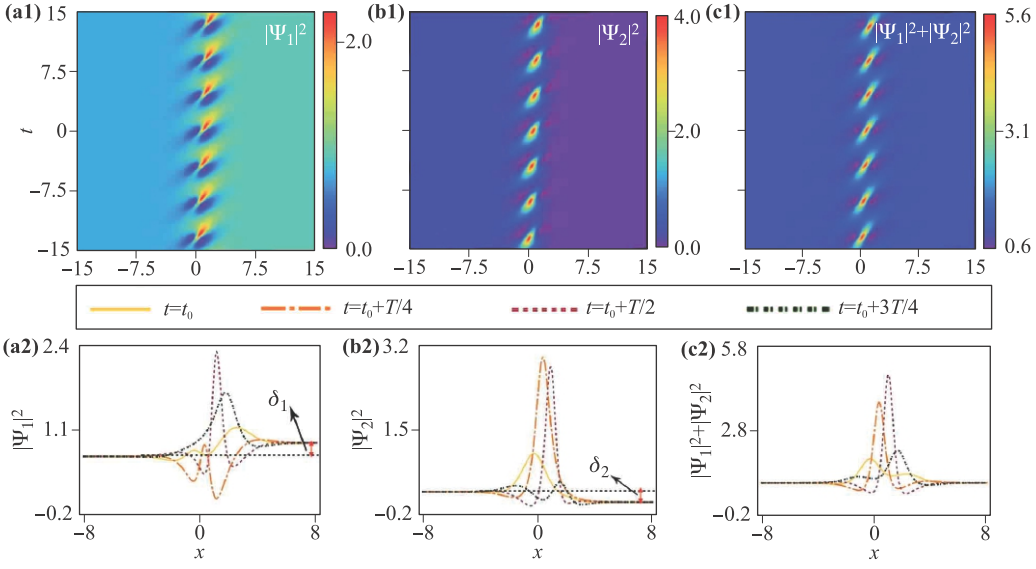

Fig. 1 Density evolutions of kink-like breathers for **(a1)** the first component, **(b1)** the second component, and **(c1)** the total density, and their corresponding density profiles within a complete period are shown in **(a2–c2)**, respectively. The parameters are $s_1=0.7125$, $s_2=0.7125$, $\omega_1=-k_{\min}$, $\omega_2=k_{\min}$, $\alpha=1$, $\kappa=0.25$, $a=-0.25$, $b=1.77$, $\alpha_0=0$, $\beta_0=\pi$.

breathers can emerge only when a certain condition is satisfied. Thus, in the next section, we will show the existence condition and dynamical characters of kink-like breathers.

3 Kink-like breathers

As we metioned before, the density distributions described by Eq. (8) may be period wave or plane wave. We would like to obtain the breathers on plane wave background, so it is instructive to consider the density distributions of the nonlinear waves, which are calculated to be the following forms:

$$|\Psi_1|^2 = [A^2 s_1^2(1+2bp_1)^2 + B^2 s_2^2(1+2bp_2)^2 + 2ABs_1 s_2(1+2bp_1)(1+2bp_2) \times \cos[(\omega_1-\omega_2)t/2 + (k_2-k_1-2k_{\min})x]/p_0^2, \tag{9}$$

$$|\Psi_2|^2 = [B^2 s_1^2(1+2bp_1)^2 + A^2 s_2^2(1+2bp_2)^2 + 2ABs_1 s_2(1+2bp_1)(1+2bp_2) \times \cos[(\omega_1-\omega_2)t/2 + (k_2-k_1-2k_{\min})x]/p_0^2. \tag{10}$$

It can be seen that the trigonometric functions in the expressions above are related to space, therefore the density distributions are spatial periodic. To make the density of background wave homogeneous, the spatially related items should be eliminated. We find that when the background wave numbers $k_{1,2}$ approach the momentum minimum $k_{\min}$ of the lowest energy states in energy–quasimomentum dispersion, namely

$$k_1 = -k_2 = -k_{\min}, \tag{11}$$

the trigonometric functions in Eqs. (9) and (10) are not related to space. Therefore the density of background become homogeneous, at the same time, the kink-like breathers emerge, as shown in Fig. 1. This kind of structure still retains the characteristics of breathers, because the periodic humps locate along the temporal dimension. But the background amplitudes on its left and right sides are quite different, which are marked as δ_1 and δ_2 in Figs. 1(a) and (b). We focus on the first component because the situation is similar to second component. In Fig. 1, the background in right side of the humps is higher than the left side in the first component, and the second component presents opposite case. Meanwhile, the total density still possesses plane wave background, as shown in Fig. 1(c). The profiles of four different moments within a complete period are shown in Figs. 1(a2)–(c2). Different from the traditional breathers, such as AB and KMB, which are always symmetric [3–6], the kink-like breathers are asymmetrical in here. We notice that a kind of similar structure was found in Ref. [48], whose background wave has a jump in the temporal direction, but its spatial distribution still possesses in the form of plane wave, that's to say, their atomic numbers have an significant transfer between two components over time. However, the background of kink-like breather in our paper exhibits the kink shape in space and can propagate in temporal direction with the kink-background form.

According to the condition (11), one can notice that the formation of kink-like breather is closely related to the strength and period of helicoidal SOC. If the background wave number and other parameters are fixed, the density distribution in Fig. 1 can be adjusted through the strength and period of the helicoidal SOC. When α is very small, there is only one valley in the first component, as shown in Fig. 2(a), in which $\alpha = 0.2$. With the strength of SOC increasing, the single valley begin to split, as shown in Fig. 2(b). And two separate valleys are formed eventually, as shown in Fig. 2(c). This splitting process can be seen more directly from the profiles in a certain moment of different values of α, as shown in Fig. 2(d). When $\alpha = 0.2$, the background difference is too small to notice, but it still exists and can be seen by comparing with the horizontal black dashed line in Fig. 2(d). Because the background wave number is fixed, when α changed, κ is actually changed. So α and κ can adjust the structure of kink-like breather together.

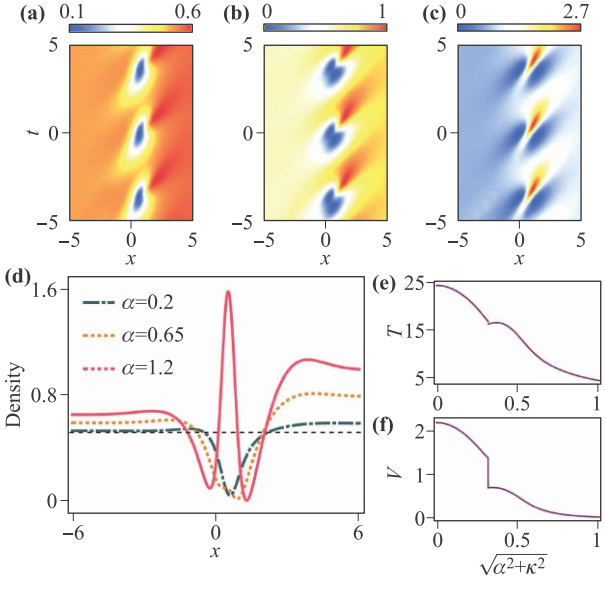

Fig. 2 Influence of α on the structure of kink-like breather. **(a–c)** The density evolution of kink-like breathers when (a) $\alpha = 0.2$ (with one valley), (b) $\alpha = 0.65$ (the intermediate state), and (c) $\alpha = 1.2$ (with two valleys). **(d)** Their corresponding profiles of density distributions, describing the splitting process from one valley to two valleys. The black dashed line is reference line. Other parameters are $s_1 = 0.7125, s_2 = 0.7125, k_1 = -k_{\min}, k_2 = k_{\min}, \kappa = \sqrt{1.2^2 - \alpha^2}, a = -0.25, b = 1.77, \alpha_0 = 0, \beta_0 = \pi$. **(e)** The dependence of kink-like breather's period on α and κ. **(f)** The dependence of kink-like breather's velocity on α and κ. α and κ are connected by $k_{\min}$.

In the previous discussions, the temporal period of the breather is metioned which can be obtained through the trigonometric function in the solution (8), i.e., $T = 4\pi/N$. Because the relationship between these parameters is too complicated, only an indirect expression of temporal period is obtained

$$T = 12\pi/\{m\kappa_3 - n[3(n_1 + n_2) - 2a - 2(k_1 + k_2)]\}.$$

The parameters involved in the expression are all related to the background wave vectors k_1 and k_2. Considering the condition (11), one can notice that the temporal period is affected by the strength and period of the helicoidal SOC. The dependence of temporal period of kink-like breather on the parameters α and κ is connected through $k_{\min}$, and the relationship is shown in Fig. 2(e). In general, the temporal period is gradually decreasing with the increase of α and κ, but there is a small increase in the process.

In addition, the spatial positions of kink-like breathers in this paper are not always stationary, but changes over time constantly, which can be seen as the velocity of kink-like breather. From the coefficients in front of x and t in the expression of ι, the velocity is calculated to be

$$\begin{aligned} v &= M/(2m) \\ &= 2(am - bn - m_1\kappa_1 + m_2\kappa_2)/[3(m_1 - m_2)]. \end{aligned}$$

Similar to the analysis of temporal period, v is also related to the parameters α and κ, and they are connected by $k_{\min}$, and the dependence is shown in Fig. 2(f). The velocity is gradually decreasing with the increase of α and κ. Here we can see that there is a sudden change in the velocity of the kink-like breather, and this unexpected change will also appear in the following-discussed characteristics of breather.

It can be seen from Fig. 2(d) that the kink amplitude (refer to the background density difference on the two sides of breathers) is smaller when α is smaller [see the green dashed line in Fig. 2(d)], and the kink amplitude seems to increase with the α increasing. In order to further explore the influence of helicoidal SOC on the structure property of kink-like breather, the kink amplitudes $\delta_{1,2}$ are calculated, which are

$$\delta_j = [\cos 2(\theta_1^+ - \theta_2^+) - \cos 2(\theta_1^- - \theta_2^-)]\frac{(-1)^j s_1 s_2 \alpha}{\sqrt{\alpha^2 + \kappa^2}}, \tag{12}$$

where $j = 1, 2$ represent the first and second component, respectively. θ_1^-, θ_1^+ are the phases of first component before and after the periodic humps emerges in Manakov system, and θ_2^+, θ_2^- are the corresponding phases of second component, and

$$\theta_1^+ = \mathrm{Arg}[\lim_{x\to+\infty} u_1] = \mathrm{Arg}[2b(E_1 - \mathrm{i}F_1)/T_1],$$

$$\theta_1^- = \mathrm{Arg}[\lim_{x\to-\infty} u_1] = \mathrm{Arg}[2b(E_2 - \mathrm{i}F_2)/T_2],$$

$$\theta_2^+ = \mathrm{Arg}[\lim_{x\to+\infty} u_2] = \mathrm{Arg}[2b(E_3 - \mathrm{i}F_3)/T_1],$$

$$\theta_2^- = \mathrm{Arg}[\lim_{x\to-\infty} u_2] = \mathrm{Arg}[2b(E_4 - \mathrm{i}F_4)/T_2].$$

It is obvious that $\delta_1 = -\delta_2$, which is intuitive, because the background of total density distribution is a plane wave. As can be seen, $\delta_{1,2}$ are directly related to the breather's initial phase difference and final phase difference between two components of the Manakov system.

The initial phase means the phase before periodic humps emerge, and final phase refers to the phase after periodic humps emerge. It has been reported that the phase of single breather structure has a shift before and after the periodic humps emerges [49]. However, the phase difference, which is closely related to the formation of kink breathers, beyond the single breath substructure and connects with the phase of two breather structures.

According to the condition (11) and the breather solution Eq. (8), we can see that the kink amplitude is related to the strength and periodic of helicoidal SOC, as well as the spectrum parameters a and b. Here we concentrate on the influence of helicoidal SOC because of their adjustability. The influence of SOC on the kink amplitude is shown in Fig. 3(a). For a certain κ, the kink amplitude always increases first, and then gradually decreases as α increases. And κ has the similar influence on the kink amplitude for a certain α. In addition, when $\alpha = 0$, no matter how κ changes, the background difference is always

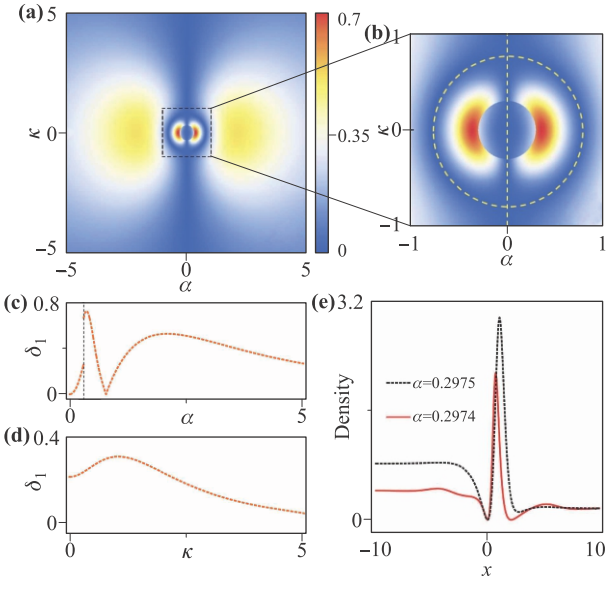

Fig. 3 **(a)** The distribution of δ_1 versus α and κ. **(b)** The enlarged square area in (a). The white dashed circle and line indicate $\delta = 0$. **(c)** The change of δ_1 versus α, where $\kappa = 0$. **(d)** The change of δ_1 versus κ, where $\alpha = 1$. **(e)** The corresponding density distribution profile before and after the kink amplitude jump. Other parameters are $s_1 = 0.7125, s_2 = 0.7125, k_1 = -k_{\min}, k_2 = k_{\min}, \alpha = 1, \kappa = 0.25, a = -0.25, b = 1.77, \alpha_0 = 0, \beta_0 = \pi$.

zero. However, when the values of α or κ fall into the area of black dashed square in Fig. 3(a), which is magnified in Fig. 3(b), the situation becomes complicated. First, there is a case of zero kink amplitude, as shown by the white dashed circle and line in Fig. 3(b). Then, if α or κ falls into the white dashed circle in Fig. 3(b), the kink amplitude increases first, and decreases to zero, then increases again and then gradually decreases. Moreover, once the value of α or κ falls into the innermost circle of Fig. 3(b), the kink amplitude jumps in its changing process, which is marked by the black dashed line in Fig. 3(c). The corresponding profiles before and after the jump are shown in Fig. 3 (e), the kink amplitude jumps so large even the amount of α changes only 0.0001.

4 The oscillation characteristics of particle number

We find that the atomic number of kink-like breather in each component oscillates with time, and the oscillation intensity can be adjusted by the helicoidal SOC. The atomic number in each component is calculated through numerical integration within a finite time, which is given by

$$N_j = \int_{-x_0-vt}^{x_0-vt} |\Psi_j|^2 \, \mathrm{d}x, \quad j = 1, 2, \tag{13}$$

where $v = M/(2m)$ is velocity of the kink-like breather. In order to ensure that the breather is always within the integration range, we choose $x_0 = 50$ and $t \in [-20, 20]$, that is enough to obtain the desired result. Generally, when $\alpha = 0$, the atomic number in each component remains constant. However, in the case of nonzero helicoidal SOC strength, such as $\alpha = 1$, the atomic number in each component fluctuates with time, but the total atomic number is constant, as shown in Fig. 4(a).

Meanwhile, the strength and period of the helicoidal SOC influence the atomic number oscillation intensity, which is described by the following quantify

$$\Delta N_j = \max[N_j] - \min[N_j], \tag{14}$$

where $j = 1, 2$ refer to the first and second components, respectively. Since the oscillation process of the two components is the same, we only consider the first component. With the α increases from 0, N_j also begins to increase from 0. after reaching an extreme value, it starts to decrease, as shown in Fig. 4(b). However, there is also an unexpected jump in $\Delta|\Psi_1|^2$, which is very similar to the jump in kink amplitude. This implies that there is a connection between kink amplitude and the intensity of atomic number oscillation. For a certain α, the effect of period of helicoidal SOC on the intensity is shown in Fig. 4(c), $\Delta|\Psi_1|^2$ decreases as the strength of helicoidal SOC increases.

The above research indicates the similar tendency of kink amplitude and the atomic number oscillation versus α and κ, i.e., they all increase first and have a jump in this process, then decrease with the increase of α and κ. Of course, the background wave number is variable with the free change of α and κ. We find that this similarity is more accordance when the background wave number is fixed. Make the background wave number fixed, then α and κ are changeable according to the condition (11). In this case, the kink amplitude and the atomic number oscillation intensity present a highly consistent tendency, as shown in Figs. 5(a) and (b). The dotted line refers to the atomic number oscillation intensity and black line indicates the kink amplitude. Even though their values are different, they still show a highly similar tendency versus α and κ. This similarity can be understood in

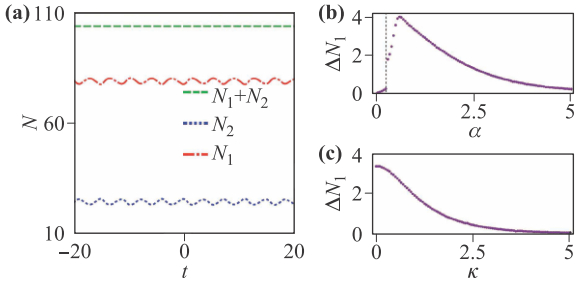

Fig. 4 **(a)** The atomic number oscillating characteristics with time in the first component (red dashing curve), the second component (blue dashing curve), and the total atomic number (green dashing curve). **(b)** The oscillating intensity of atomic number versus α, when $\kappa = 0$. **(c)** The oscillating intensity of atomic number versus κ, when $\alpha = 1$. Other parameters are $s_1 = 0.7125, s_2 = 0.7125, k_1 = -k_{\min}, k_2 = k_{\min}, \alpha = 1, \kappa = 0.25, a = -0.25, b = 1.77, \alpha_0 = 0, \beta_0 = \pi$.

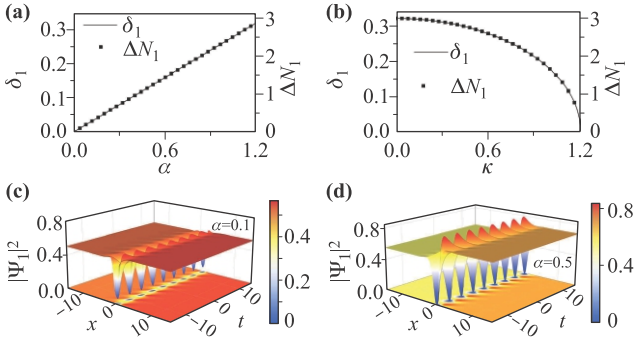

Fig. 5 **(a, b)** Dependences of the kink amplitude δ_1 (solid curve) and the oscillating amplitude of atomic number ΔN_j (square points) on (a) α and (b) κ. **(c, d)** Density evolution of breathers of the first component, $\alpha = 0.1$ in (c) and $\alpha = 0.5$ in (d). The parameters are $s_1 = 0.7125, s_2 = 0.7125, k_1 = -1.2, k_2 = 1.2, a = -0.25, b = 1.77, \alpha_0 = 0, \beta_0 = \pi$.

the following manner, the kink amplitude can affect the atomic number oscillate intensity. For a certain background wave number, a small SOC strength corresponds to small kink amplitude, and in the process of kink amplitude growth with the helicoidal SOC, the atomic number oscillation intensity also growing, and the higher kink amplitude induces a more drastic oscillate intensity, and they all exhibit a direct proportion relationship. As shown in Figs. 5(c) and (d), the background wave number is fixed as $k_1 = -k_2 = 1.2$. When $\alpha = 0.1$, the density distribution is shown in Fig. 5(c). The density distribution with a significant enhancement is shown in Fig. 5(d), where $\alpha = 0.5$. This contrast of breathing intensity is particularly obvious in the first component. While, the kink amplitude of second component is too small to be obvious and they are not shown in here. It can be seen from Fig. 5(a) as well as Eq. (12), when $\alpha = 0.1$, the kink amplitude is nearly 0.03; when $\alpha = 0.5$, δ_1 is nearly 0.16, but the peaks value for second component are both much bigger than these two values of kink amplitude, so the kink amplitude is too small to be obvious.

In addition, we consider the stability of the kink-like breathers described by Eq. (7). Because the density distribution of breather usually changing with time, the methods like Bogoliubov analysis are no longer applicable. So, the numerical simulation is considered. In our numerical simulation, the states of $t = 2$ of Eq. (7) are chosen to be the initial states, because the breathers shape change smoothly at this moment. At the same time, a random noise with amplitude 0.001 is added. The breathers at different strength and period of helicoidal SOC are simulated, and their density evolution are shown in Fig. 6. It can be seen that the breather can maintain stable oscillation and evolve for several temporal periods. The results in here can show the robustness of kink-like breathers.

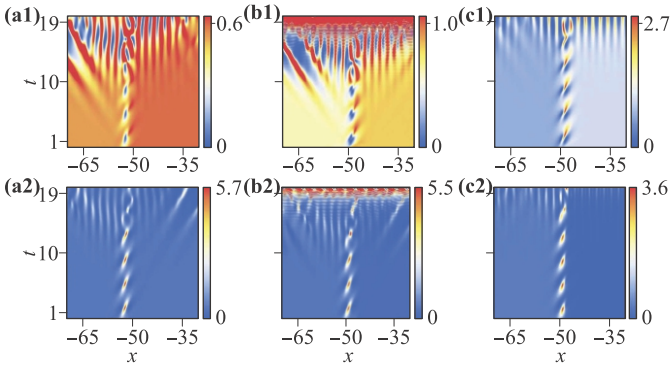

Fig. 6 The density distributions of kink-like breathers obtained through numerical simulation under random noises. **(a1–c1)** The density distributions for first component, where $\alpha = 0.2, \alpha = 0.65, \alpha = 1.2$ respectively. **(a2–c2)** The corresponding density distributions for the second component. Other parameters are $s_1 = 0.7125, s_2 = 0.7125, k_1 = -1.2, k_2 = 1.2, a = -0.25, b = 1.77, \alpha_0 = 0, \beta_0 = \pi$.

5 Discussion and conclusion

In summary, the kink-like breather is found in BECs with helicoidal SOC, which is described by the exact analytical solution. The solution is transformed from the breather solution of Manakov system. Then, the kink-like breather emerges only when the condition (11) is satisfied, where the background wave number and the momentum minimum of lowest energy states are connected. The kink amplitude, which is defined by the background's density difference on the kink-like breather's two sides, is related to the phase difference of before-transformed solution. Meanwhile,The strength and period of SOC affect the kink amplitude and shape, as well as temporal period and velocity of this kind of breather. With the strength of SOC increasing, the one valley of breather in first component splits into two valleys gradually. It is worth mentioning that there is a jump when the kink amplitude increases with the strength and period of the helicoidal SOC. The oscillating characteristics of atomic number have also been researched, and it presents similar tendencies with the kink amplitude versus the helicoidal SOC. This similarity is more consistent when the background wave number is fixed. And the breathing intensity of kink-like breathers can be controlled by adjusting their kink amplitude. The stability of the found solutions are tested through the numerical simulation. In the simulation, kink-like breathers are stable within several temporal periods, which can indicate the robustness of the breathers. The kink-like breathers in BECs with helicoidal SOC enrich our understanding on the generations of new kinds of nonlinear waves. Only one dimensional BEC is considered in here, in fact, nonlinear waves, such as soliton, display much more special states in two dimensional BEC with helicoidal SOC [34]. So it will be interesting to research breathers in these systems in the future.

Acknowledgements This work was supported by the National Natural Science Foundation of China (Grant Nos. 11875220, 12047502, and 12022513).

References

1. M. Matuszewski, E. Infeld, B. A. Malomed, and M. Trippenbach, Fully three dimensional breather solitons can be created using Feshbach resonances, *Phys. Rev. Lett.* 95(5), 050403 (2005)
2. M. Yu, J. K. Jang, Y. Okawachi, A. G. Griffith, K. Luke, S. A. Miller, X. Ji, M. Lipson, and A. L. Gaeta, Breather soliton dynamics in microresonators, *Nat. Commun.* 8(1), 14569 (2017)
3. D. Luo, Y. Jin, J. H. V. Nguyen, B. A. Malomed, O. V. Marchukov, V. A. Yurovsky, V. Dunjko, M. Olshanii, and R. G. Hulet, Creation and characterization of matter-wave breathers, *Phys. Rev. Lett.* 125(18), 183902 (2020)

4. E. A. Kuznetsov, Solitons in parametrically unstable plasma, *Dokl. Akad. Nauk SSSR* 236, 575 (1977)
5. Y. C. Ma, The perturbed plane-wave solutions of the cubic Schrödinger equation, *Stud. Appl. Math.* 60(1), 43 (1979)
6. N. N. Akhmediev and V. I. Korneev, Modulation instability and periodic solutions of the nonlinear Schrödinger equation, *Theor. Math. Phys.* 69(2), 1089 (1986)
7. M. Tajiri and Y. Watanabe, Breather solutions to the focusing nonlinear Schrödinger equation, *Phys. Rev. E* 57(3), 3510 (1998)
8. C. Liu and N. Akhmediev, Super-regular breathers in nonlinear systems with self-steepening effect, *Phys. Rev. E* 100(6), 062201 (2019)
9. C. Liu, Z. Y. Yang, and W. L. Yang, Growth rate of modulation instability driven by superregular breathers, *Chaos* 28(8), 083110 (2018)
10. Y. H. Wu, C. Liu, Z. Y. Yang, and W. L. Yang, Breather interaction properties induced by self-steepening and space–time correction, *Chin. Phys. Lett.* 37(4), 040501 (2020)
11. N. Akhmediev, J. M. Soto-Crespo, and A. Ankiewicz, How to excite a rogue wave, *Phys. Rev. A* 80(4), 043818 (2009)
12. B. Frisquet, B. Kibler, and G. Millot, Collision of Akhmediev breathers in nonlinear fiber optics, *Phys. Rev. X* 3(4), 041032 (2013)
13. F. Baronio, A. Degasperis, M. Conforti, and S. Wabnitz, Solutions of the vector nonlinear schrödinger equations: Evidence for deterministic rogue waves, *Phys. Rev. Lett.* 109(4), 044102 (2012)
14. B. Kibler, J. Fatome, C. Finot, G. Millot, F. Dias, G. Genty, N. Akhmediev, and J. M. Dudley, The Peregrine soliton in nonlinear fibre optics, *Nat. Phys.* 6(10), 790 (2010)
15. H. Bailung, S. K. Sharma, and Y. Nakamura, Observation of peregrine solitons in a multicomponent plasma with negative ions, *Phys. Rev. Lett.* 107(25), 255005 (2011)
16. A. Chabchoub, N. P. Hoffmann, and N. Akhmediev, Rogue wave observation in a water wave tank, *Phys. Rev. Lett.* 106(20), 204502 (2011)
17. C. Liu, Z. Y. Yang, L. C. Zhao, and W. L. Yang, Vector breathers and the inelastic interaction in a three-mode nonlinear optical fiber, *Phys. Rev. A* 89(5), 055803 (2014)
18. C. Liu, Z. Y. Yang, W. L. Yang, and N. Akhmediev, Chessboard-like spatio-temporal interference patterns and their excitation, *J. Opt. Soc. Am. B* 36(5), 1294 (2019)
19. M. H. Anderson, J. R. Ensher, M. R. Matthews, C. E. Wieman, and E. A. Cornell, Observation of Bose–Einstein condensation in a dilute atomic vapor, *Science* 269(5221), 198 (1995)
20. Y. Zhang, M. E. Mossman, T. Busch, P. Engels, and C. Zhang, Properties of spin–orbit-coupled Bose–Einstein condensates, *Front. Phys.* 11(3), 118103 (2016)
21. Y. J. Lin, K. Jiménez-García, and I. B. Spielman, Spin–orbit-coupled Bose–Einstein condensates, *Nature* 471, 83 (2011)
22. J. Dalibard, F. Gerbier, G. Juzeliūnas, and P. Öhberg, Colloquium: Artificial gauge potentials for neutral atoms, *Rev. Mod. Phys.* 83(4), 1523 (2011)
23. Y. Xu, Y. Zhang, and B. Wu, Bright solitons in spin–orbit-coupled Bose–Einstein condensates, *Phys. Rev. A* 87(1), 013614 (2013)
24. V. Achilleos, D. J. Frantzeskakis, P. G. Kevrekidis, and D. E. Pelinovsky, Matter-wave bright solitons in spin–orbit coupled Bose–Einstein condensates, *Phys. Rev. Lett.* 110(26), 264101 (2013)
25. V. Achilleos, J. Stockhofe, P. G. Kevrekidis, D. J. Frantzeskakis, and P. Schmelcher, Matter-wave dark solitons and their excitation spectra in spin–orbit coupled Bose–Einstein condensates, *EPL* 103(2), 20002 (2013)
26. V. Achilleos, D. J. Frantzeskakis, P. G. Kevrekidis, P. Schmelcher, and J. Stockhofe, Positive and negative mass solitons in spin–orbit coupled Bose–Einstein condensates, arXiv: 1502.05574 (2015)
27. L. C. Zhao, X. W. Luo, and C. Zhang, Magnetic stripe soliton and localized stripe wave in spin-1 Bose–Einstein condensates, *Phys. Rev. A* 101(2), 023621 (2020)
28. Y. V. Kartashov and V. V. Konotop, Solitons in Bose–Einstein condensates with helicoidal spin–orbit coupling, *Phys. Rev. Lett.* 118(19), 190401 (2017)
29. Y. A. Bychkov and E. I. Rashba, Oscillatory effects and the magnetic susceptibility of carriers in inversion layers, *J. Phys. C* 17(33), 6039 (1984)
30. G. Dresselhaus, Spin–orbit coupling effects in zinc blende structures, *Phys. Rev.* 100(2), 580 (1955)
31. X. W. Luo, K. Sun, and C. Zhang, Spin-tensor-momentum-coupled Bose–Einstein condensates, *Phys. Rev. Lett.* 119(19), 193001 (2017)
32. R. X. Zhong, Z. P. Chen, C. Q. Huang, Z. H. Luo, H. S. Tan, B. A. Malomed, and Y. Y. Li, Self-trapping under two-dimensional spin–orbit coupling and spatially growing repulsive nonlinearity, *Front. Phys.* 13(4), 130311 (2018)
33. S. W. Song, L. Wen, C. F. Liu, S. C. Gou, and W. M. Liu, Ground states, solitons and spin textures in spin-1 Bose–Einstein condensates, *Front. Phys.* 8(3), 302 (2013)
34. Y. V. Kartashov, E. Y. Sherman, B. A. Malomed, and V. V. Konotop, Stable two-dimensional soliton complexes in Bose–Einstein condensates with helicoidal spin–orbit coupling, *New J. Phys.* 22(10), 103014 (2020)
35. G. H. Chen, H. C. Wang, Z. P. Chen, and Y. Liu, Fundamental modes in waveguide pipe twisted by saturated double-well potential, *Front. Phys.* 12(1), 124201 (2017)
36. K. Jiménez-García, L. J. LeBlanc, R. A. Williams, M. C. Beeler, C. Qu, M. Gong, C. Zhang, and I. B. Spielman, Tunable spin–orbit coupling via strong driving in ultracold-atom systems, *Phys. Rev. Lett.* 114(12), 125301 (2015)
37. X. Luo, L. Wu, J. Chen, Q. Guan, K. Gao, Z. F. Xu, L. You, and R. Wang, Tunable atomic spin–orbit coupling synthesized with a modulating gradient magnetic field, *Sci. Rep.* 6(1), 18983 (2016)

38. S. Manakov, On the theory of two-dimensional stationary self-focusing electromagnetic waves, *J. Exp. Theor. Phys.* 38, 248 (1974)
39. Y. Li, L. P. Pitaevskii, and S. Stringari, Quantum tricriticality and phase transitions in spin–orbit coupled Bose–Einstein condensates, *Phys. Rev. Lett.* 108(22), 225301 (2012)
40. Y. Yang, P. Gao, Z. Wu, L. C. Zhao, and Z. Y. Yang, Matter-wave stripe solitons induced by helicoidal spin–orbit coupling, *Ann. Phys.* 431, 168562 (2021)
41. B. Guo, L. Ling, and Q. P. Liu, Nonlinear Schrödinger equation: Generalized Darboux transformation and rogue wave solutions, *Phys. Rev. E* 85(2), 026607 (2012)
42. C. Liu and N. Akhmediev, Super-regular breathers in nonlinear systems with self-steepening effect, *Phys. Rev. E* 100(6), 062201 (2019)
43. L. Duan, Z. Y. Yang, P. Gao, and W. L. Yang, Excitation conditions of several fundamental nonlinear waves on continuous-wave background, *Phys. Rev. E* 99(1), 012216 (2019)
44. L. C. Zhao and J. Liu, Localized nonlinear waves in a two-mode nonlinear fiber, *J. Opt. Soc. Am. B* 29(11), 3119 (2012)
45. L. Ling, L. C. Zhao, and B. Guo, Darboux transformation and multi-dark soliton for *N*-component nonlinear Schrödinger equations, *Nonlinearity* 28(9), 3243 (2015)
46. L. C. Zhao, C. Liu, and Z. Y. Yang, The rogue waves with quintic nonlinearity and nonlinear dispersion effects in nonlinear optical fibers, *Commun. Nonlinear Sci. Numer. Simul.* 20, 1007 (2014)
47. Y. H. Qin, Y. Wu, L. C. Zhao, and Z. Y. Yang, Interference properties of two-component matter wave solitons, *Chin. Phys. B* 29(2), 020303 (2020)
48. L. Ling and L. C. Zhao, Integrable pair-transition-coupled nonlinear Schrödinger equations, *Phys. Rev. E* 92(2), 022924 (2015)
49. N. Devine, A. Ankiewicz, G. Genty, J. M. Dudley, and N. Akhmediev, Recurrence phase shift in Fermi–Pasta–Ulam nonlinear dynamics, *Phys. Lett. A* 375, 4158 (2011)